

Instability of particle inertial migration in shear flow

Evgeny S. Asmolov,^{1,2} Tatiana V. Nizkaya,¹ Jens Harting,^{3,4} and Olga I. Vinogradova^{1, a)}

¹⁾ *Frumkin Institute of Physical Chemistry and Electrochemistry, Russian Academy of Science, 31 Leninsky Prospect, 119071 Moscow, Russia*

²⁾ *Institute of Mechanics, Lomonosov Moscow State University, 119991 Moscow, Russia*

³⁾ *Helmholtz Institute Erlangen-Nürnberg for Renewable Energy, Forschungszentrum Jülich, Cauerstrasse 1, 91058 Erlangen, Germany*

⁴⁾ *Department of Chemical and Biological Engineering and Department of Physics, Friedrich-Alexander-Universität Erlangen-Nürnberg, Cauerstrasse 1, 91058 Erlangen, Germany*

(Dated: July 16, 2021)

In a shear flow particles migrate to their equilibrium positions in the microchannel. Here we demonstrate theoretically that if particles are inertial, this equilibrium can become unstable due to the Saffman lift force. We derive an expression for the critical Stokes number that determines the onset of instable equilibrium. We also present results of lattice Boltzmann simulations for spherical particles and prolate spheroids to validate the analysis. Our work provides a simple explanation of several unusual phenomena observed in earlier experiments and computer simulations, but never interpreted before in terms of the instable equilibrium.

I. INTRODUCTION

In shear flows particles experience an inertial lift force which induces their migration across streamlines. This effect was first discovered for neutrally buoyant particles in tubes¹ and is currently widely employed to separate particles in microfluidic devices². In an unbounded shear flow, the Saffman lift force³ emerges when a slip velocity (i.e. a difference between particle velocity and fluid velocity at the particle center) becomes finite. The disturbance of the flow in this case is caused by a streamwise drag force and momentum released into the fluid. In the channel (wall-bounded) flows, another type of the lift force emerges for a freely rotating and translating particle. Namely, a neutrally buoyant lift force^{4,5}, which is due to the curvature of the undisturbed velocity profile or wall effects.

The inertial migration of particles is traditionally considered as a quasi-steady process. This implies that the particle inertia is neglected, so that hydrodynamic forces (the drag, the neutrally buoyant lift, the Dean force⁶) as well as any external forces are balanced, i.e. $\mathbf{F}(\mathbf{x}_p, \mathbf{V}, \mathbf{U}) = 0$, where \mathbf{x}_p and \mathbf{V} are the particle position and velocity, correspondingly, and \mathbf{U} is the fluid velocity. Besides, it is commonly considered that the Saffman lift emerges only under forces acting in the streamwise direction (e.g. non-neutrally buoyant particles under gravity in vertical channels). Such a quasi-steady approach allows one to infer the particle velocity $\mathbf{V}(\mathbf{x})$ by using the lift and drag coefficients. Since the drag coefficient is positive-definite, the behavior of the particle is controlled by the variation of the lift force across the channel: the zeros of the lift force correspond to the particle equilibrium positions and its gradients

define their stability. In computer simulations, the lift force on a particle at different positions can be measured independently and is often used to predict the particle behavior⁷. By contrast, direct experimental measurements of the lift force are impossible. This force is usually calculated from the measured migration velocity⁸.

The particle inertia is characterized by the Stokes number $St = 2\rho_p Re_G / (9\rho)$, where ρ_p and ρ are the particle and fluid densities, $Re_G = Ga^2/\nu$ is the particle Reynolds number defined using the particle radius a , shear rate G and kinematic viscosity of the fluid ν . Clearly, at sufficiently large Re_G the Stokes number can become finite even for neutrally buoyant particles with $\rho_p/\rho = 1$. Consequently, when such particles migrate across the streamlines, they accelerate by the fluid. In this case, the momentum exchange between the fluid and the particle generates the Saffman lift force, and the quasi-steady approach is no longer applicable.

Despite this obvious fact, the correctness of the quasi-steady approach at $Re_G > 1$ is still not under dispute, and migration phenomena are commonly analyzed in terms of the dependence of the lift force on the particle position, its zeros and their bifurcations^{7,9}. As one example, numerous experiments with neutrally buoyant particles in circular tubes found that at high channel Reynolds numbers the Segre-Silberberg equilibrium position shifts towards the wall, but some particles migrate towards the center to form an inner annulus¹⁰⁻¹². However, their interpretation implies that in the long run all particles will focus at the zeros of the lift curve, although note that there have been some suggestions that the inner annulus is a second “true” equilibrium position^{10,12} or represents only a transient configuration¹¹. Another example refers to the computer simulations of the inertial behavior of spheroids in shear flow that is currently a subject of active research¹³⁻¹⁶. It is well known that at large Re_G and St prolate spheroids undergo a series of transitions between different rotational regimes. All

^{a)}Corresponding author: oivinograd@yahoo.com

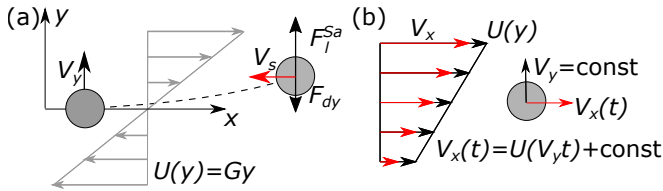


Figure 1. (a) Sketch of the particle motion in a shear flow. A particle translating across the streamlines experiences a transverse drag F_{dy} and a lift force F_l^{Sa} . (b) Particle velocity in a neutral equilibrium.

these studies assume that spheroids move with the velocity of the fluid that is equivalent to a decoupling between rotational and translational motion. This, in turn, implies that the equilibrium is always stable, which is by no means obvious at large St .

In the present paper, we analyse the equilibrium state of torque- and force-free spherical particles in the shear flow. We show that at finite St this equilibrium becomes unstable due to the Saffman lift force. Using lattice Boltzmann simulations we then verify our theoretical predictions for spheres and prolate spheroids.

Our paper is organized as follows. In Sec. II we derive equations of the particle motion in an unbounded shear flow and obtain a stability criterion for small Re_G and finite St . In Sec. III we show how particle inertia and Saffman lift modify the particle migration velocity under a transverse force in wall-bounded flows. The lattice Boltzmann method is described in Sec. IV. In Sec. V we present the simulation results that validate our theoretical predictions for heavy spheres and prolate spheroids at finite Re_G . Our conclusions are summarized in Sec. VI. Appendix A generalizes the Saffman formula to the case of a particle translating in a transverse direction with a constant velocity and accelerating in a streamwise direction.

II. STABILITY OF PARTICLE MOTION IN AN UNBOUNDED SHEAR FLOW

We begin with the migration of a force- and torque-free spherical particle of radius a and density ρ_p in an unbounded linear shear flow, $\mathbf{U}' = U' \mathbf{e}_x$, $U' = Gy$ where \mathbf{e}_x is the unit vector along the x -axis (see Fig. 1 (a)). The particle Reynolds number $Re_G = \rho Ga^2/\mu$ is finite, where ρ and μ are the fluid density and viscosity. The initial particle position is $\mathbf{x}'_{p0} = (x'_{p0}, y'_{p0}, z'_{p0}) = \mathbf{0}$.

The equations of particle motion in dimensional variables read

$$m \frac{d\mathbf{V}'}{dt'} = \mathbf{F}', \quad (1)$$

$$\frac{d\mathbf{x}'_p}{dt'} = \mathbf{V}', \quad (2)$$

where $m = 4/3\pi\rho_p a^3$ is the particle mass, $\mathbf{V}' = (V'_x, V'_y)$ is the particle translational velocity, and $\mathbf{F}' = (F'_x, F'_y) = \mathbf{F}'_d + \mathbf{F}'_t + \mathbf{F}'_l^{Sa}$ is the hydrodynamic force. Here, \mathbf{F}'_d is the quasi-steady drag force and \mathbf{F}'_t is an unsteady force due to particle acceleration which includes the Basset and added-mass forces¹⁷. The Saffman lift force $\mathbf{F}'_l^{Sa} = F'_l^{Sa} \mathbf{e}_y$ is proportional to the momentum released by the particle into shear flow. Note that we do not include the equation for the rotational velocity since it has little effect on the sphere's dynamics in shear flows¹⁸.

A steady-state solution of Eqs.(1) and (2) in the absence of external force is

$$\mathbf{V}'_0 = \mathbf{0}, \quad \mathbf{x}'_{p0} = \mathbf{0}. \quad (3)$$

To distinguish between the stable and unstable equilibrium states we employ the linear stability analysis. Let us consider how the particle at the equilibrium position reacts to a small disturbance in the initial velocity. For small (slip Reynolds number) $Re_V = a|\mathbf{V}' - \mathbf{U}'(y_p)|/\nu$ Eqs.(1) and (2) can be linearized by expanding \mathbf{V}' . The drag force then takes the form $F'_{dx} = -6\pi\mu a f_x (V'_x - Gy'_p)$, $F'_{dy} = -6\pi\mu a f_y V'_y$, where $f_x(Re_G)$ and $f_y(Re_G)$ are the correction factors accounting for the effect of fluid inertia at finite Re_G . At small Re_G they converge to unity.

It is now convenient to introduce dimensionless variables by scaling the velocities by Ga , the coordinates by a , the time by G^{-1} , and the forces by $6\pi\mu a^2 G$. The linearized equations can then be formulated as

$$St \frac{dV'_x}{dt} = -f_x (V'_x - y_p) + F'_{tx}, \quad (4)$$

$$St \frac{dV'_y}{dt} = -f_y V'_y + F'_l^{Sa} + F'_{ty}, \quad (5)$$

$$\frac{dy_p}{dt} = V'_y, \quad (6)$$

where St is the Stokes number,

$$St = \frac{2\rho_p Ga^2}{9\mu} = \frac{2\rho_p}{9\rho} Re_G. \quad (7)$$

The origin of instability can be understood as follows. Assume a small disturbance of the particle from its equilibrium position leading to a positive transverse velocity V'_y (see Fig. 1(a)). The emerging negative transverse drag $F'_{dy} = -f_y V'_y < 0$ should tend to stop the particle. However, since the particle enters the region of a larger fluid velocity, it lags behind the fluid due to its inertia. The particle that is subject to a drag force, $F'_{dx} = -f_x V'_s > 0$, where $V'_s = V'_x - y_p < 0$ is the slip velocity, begins to accelerate in the streamwise direction. This, in turn, should induce a positive Saffman lift force $F'_l^{Sa} > 0$ which may exceed the transverse drag by leading to further acceleration of the particle in the transverse direction. We refer this situation to as unstable.

By contrast, when the equilibrium is neutral, which implies that small disturbances neither grows nor disappear, V'_y and V'_s are constant (see Fig. 1(b)). The acceleration of a particle is also constant and equal to the fluid

acceleration along its trajectory

$$\frac{dV_x}{dt} = V_y \frac{dU}{dy} \mathbf{e}_x = V_y \mathbf{e}_x = \text{const.} \quad (8)$$

It follows from Eq. (5) that if $dV_y/dt = 0$, the unsteady force F_{ty} and the inertia term in the left-hand side vanish. The condition of a neutral equilibrium can then be formulated as

$$F_l^{Sa} - f_y V_y = 0. \quad (9)$$

To apply the criterion (9) it is necessary to calculate the lift force F_l^{Sa} for the neutral equilibrium, which is not straightforward. In the classical Saffman theory³ the lift force is proportional to (constant) V_s . In our case the situation is different since the particle accelerates in the streamwise direction, and the lift force is related to the particle acceleration given by Eq.(A6) (see Appendix A for a derivation) as

$$F_l^{Sa} = C_l^{Sa} \text{St} V_y \quad \text{as} \quad \text{Re}_V \ll \text{Re}_G \ll 1. \quad (10)$$

Here $C_l^{Sa} = 0.343 \text{Re}_G^{1/2}$ is the Saffman lift coefficient, which characterizes the lift-to-drag ratio. One can expect that the lift force at finite Re_G is described by (10), i.e.

$$F_l^{Sa} = C_l \text{St} V_y \quad \text{as} \quad \text{Re}_V \ll 1, \quad (11)$$

but $C_l \neq C_l^{Sa}$ and its dependence on Re_G has to be calculated.

By balancing the lift (Eq.(11)) and the transverse drag (Eq.(5)) forces, we can find the critical Stokes number

$$\text{St}_{cr} = \frac{f_y}{C_l}, \quad (12)$$

which determines the onset of the unstable equilibrium. For $\text{St} < \text{St}_{cr}$ the equilibrium is stable, but when $\text{St} > \text{St}_{cr}$, the lift force becomes larger than the transverse drag, $F_l^{Sa} > f_y V_y$, and the unstable regime develops. Note that at small Re_G the value of C_l can be found using (A4), and the correction factor is $f_y = 1$. Therefore, in this limiting case $\text{St}_{cr} = 2.92 \text{Re}_G^{-1/2}$.

Eq.(7) can be used to reformulate Eq. (12) as

$$\left[\frac{9f_y}{2\text{Re}_G C_l} \right]_{cr} = \frac{\rho_p}{\rho}. \quad (13)$$

This equation can be seen as an implicit condition on the critical Reynolds number. Thus, when the Saffman theory is valid, using Eq. (A4) one can obtain from (13) that

$$\text{Re}_{cr} = 5.56 \left(\frac{\rho_p}{\rho} \right)^{-2/3} \ll 1 \quad \text{as} \quad \rho_p/\rho \gg 1. \quad (14)$$

It indicates that at a large density ratio, e.g. for aerosol particles the critical Reynolds numbers is small. Say, for water droplets in air ($\rho_p/\rho \simeq 800$) the instability is expected at $\text{Re}_G > \text{Re}_{cr} \simeq 0.065$.

For smaller density ratios, including $\rho_p/\rho = 1$ (neutrally buoyant particles), the instability should also occur, but at finite Re_G . To generalize the scaling equation (14) to the case of finite Re_G we have to calculate $f_y(\text{Re}_G)$ and $C_l(\text{Re}_G)$. Moreover, in practice we normally deal with a wall-bounded flow, termed the Couette flow, where these coefficients depend on the channel thickness.

III. PARTICLE MIGRATION UNDER A TRANSVERSE FORCE

The theoretical model described above corresponds to an idealized situation of migration in an unbounded shear flow and without external forces acting. In this Section we consider the channel flow, where the interactions with the walls should be taken into account. Besides, the particle may also experience an extra transverse force $F_{ex} \mathbf{e}_y$ induced by external fields (gravitational, electric, magnetic) or an additional hydrodynamic force, such as, for example, the Dean force (in curved channels) or the so-called neutrally buoyant lift force F_l^{nb} .

The force F_l^{nb} is usually evaluated numerically, assuming that the particle is free to rotate and move in the x -direction, but is fixed in the transverse direction¹⁹⁻²¹. Then, inertial migration of a particle to its equilibrium position is simulated by balancing the lift force F_l^{nb} and the transverse drag, i.e. the Saffman lift force F_l^{Sa} is neglected although it can be significant at finite Re_G .

Let us now generalize our analysis of instability to the case of a finite transverse force $F_{ex}(y_p)$ which depends only on the particle position y_p , but not on its migration velocity V_y . We make an additional assumption that the Reynolds number Re_V is small and the force changes slowly during particle migration, i.e. the characteristic migration time $H/|V_y|$ is large compared to the hydrodynamic time scale G^{-1} . Here H is the characteristic length scale for the change of F_{ex} (that is usually the channel width). This is justified, i.e. the ratio of the two time scales is large, provided particles are small

$$\frac{GH}{|V_y|} = \frac{\text{Re}_G H}{\text{Re}_V a} \gg 1 \quad \text{as} \quad a/H \ll 1, \quad \text{Re}_V \ll \text{Re}_G.$$

In this case the migration is quasi-steady so that the acceleration term in Eq. (5) can be ignored as in the neutral stability regime. We further assume that the Saffman lift F_l^{Sa} is controlled by streamwise acceleration of the particle due to its transverse motion, i.e. given by (10). For such a situation Eq.(5) for the transverse momentum can be rewritten as

$$0 = -f_y(y_p) V_y + C_l(y_p) \text{St}(y_p) V_y + F_{ex}(y_p), \quad (15)$$

where the Stokes number is based on a local shear rate $G(y_p)$, and the coefficients f_y and C_l should depend on the location of the particle to account for hydrodynamic interactions with the walls.

Eq. (15) allows one to obtain the migration velocity under a slowly varying transverse force F_{ex} :

$$V_y = \frac{F_{ex}}{f_y - C_l \text{St}}. \quad (16)$$

We recall that the migration velocity is usually determined by balancing F_{ex} and $F_{dy} = f_y V_y$, so that $V_{y0} = F_{ex}/f_y$. Since for neutrally buoyant particles it is traditionally assumed that $f_y = 1$, the migration velocity is simply $V_{y0} = F_l^{nb}$.^{19–21} Our results, however, show that due to the effect of the Saffman lift force V_y significantly deviates from V_{y0} , especially when the denominator in (16) is small.

If we consider a small perturbation δV_y of the quasi-steady velocity (16), one can find that transverse motion becomes unstable when $C_l(y_p) \text{St}(y_p) - f_y(y_p) > 0$. Therefore, we recover the stability criterion (12) for the force-free case, but now it involves functions of y_p . This suggests that the motion can be unstable only in some parts of the channel.

Eq.(16) for the migration velocity can be rewritten as

$$V_y = \frac{F_{ex}}{f_y (1 - \text{Re}_G/\text{Re}_{cr})}, \quad (17)$$

which includes Re_{cr} . The last equation should be used for interpreting experimental data on migration velocity. One can also conclude that the application of a steady state model to calculate the lift force from data obtained at finite Re_G can strongly overestimate the result, and would also lead to incorrect scaling relationships.

IV. SIMULATION METHOD

To simulate the flow we use a 3D implementation of the lattice Boltzmann method (LBM) with a 19 velocity, single relaxation time scheme and the Batnagar Gross Krook (BGK) collision operator^{22,23}. Particles are discretized on the fluid lattice and implemented as moving no-slip boundaries following Ladd²⁴. The relaxation time of the BKG collision operator is fixed to unity leading to a kinematic viscosity of $\nu = 1/6$. Here and below the variables are given in simulation units. In addition, we set the fluid density $\rho = 1$. Further implementation details are provided in our previous publications^{23,25–29}.

The size of the computational domain in most simulations is $(N_x, N_y, N_z) = (200, 161, 100)$. We used spherical particles with radius $a = 8$, which provides $H/a \simeq 20$, and prolate spheroids with equatorial radius $a = 4$ and polar radius $b = 8$. To generate a shear flow we implement impermeable no-slip walls moving with opposite velocities (V_w at the top wall and $-V_w$ at the bottom wall)³⁰ and impose periodic boundary conditions in the other two directions. The generated shear rate in simulation units is $G = 2V_w/(N_y - 1)$.

To search the unstable regimes for the particle equilibrium position at the channel mid-plane we vary Re_G

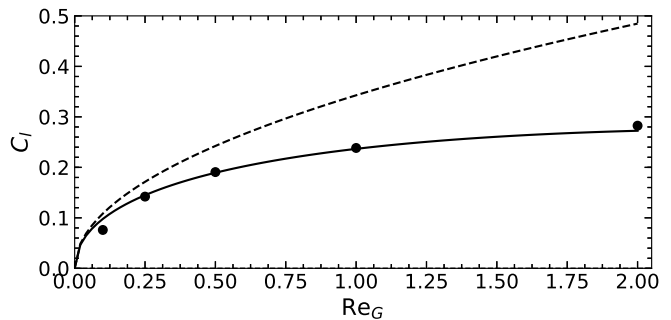


Figure 2. Lift-to-drag ratio for a particle translating with a small slip velocity (slip Reynolds number $\text{Re}_V = 0.05$) along the mid-plane. Circles show the simulation results. The dashed and solid curves are calculations from Eq.(A4) and Eq.(18).

in the range from 0.25 to 2 and the particle density ρ_p in the range from 15 to 200 to obtain different values of the Stokes number St . We set initial rotational velocity $\omega_z = -G/2$ and translational velocity $\mathbf{V} = (0.1Ga, 0, 0)$, and fix the transverse coordinate $y_p = 0$ during 3×10^4 time steps, waiting for the system to equilibrate. Then, we release the particle and track its position for $\sim 10^5$ time steps. If the transverse coordinate y_p grows with time exponentially the equilibrium is deemed unstable.

V. RESULTS AND DISCUSSION

It is of considerable interest to compare LBM simulation data with our analytical theory and to determine the regimes of validity of the theoretical results. Here we present results of our simulations together with specific calculations using theoretical expressions.

A. Lift-to-drag ratio and transverse drag

According to Eq.(12) the critical Stokes number that should give us the instability onset depends on the ratio of C_l and f_y . We, therefore, begin with the investigation of these parameters.

To obtain the dependence of C_l on Re_G we put the particle at the mid-plane of the channel and then move it in the x -direction with a velocity V_x that corresponds to fixed $\text{Re}_V = 0.05$. By setting different V_w we vary Re_G from 0.1 to 2. After equilibration, i.e. when the rotational velocity of the particle becomes stationary, we measure the lift (F_l^{Sa}) and drag (F_{dx}) forces on the particle and average them over 10^4 time steps. Then the lift-to-drag ratio is calculated as $C_l = F_l^{Sa}/F_{dx}$. We remark that in these simulations we use our standard box that gives $H/a = 20$, but we have verified that the results for C_l do not change if we set $H/a = 40$.

The computed lift-to-drag ratio $C_l = F_l^{Sa}/F_{dx}$ as a function of Re_G is shown in Fig. 2. We see that on

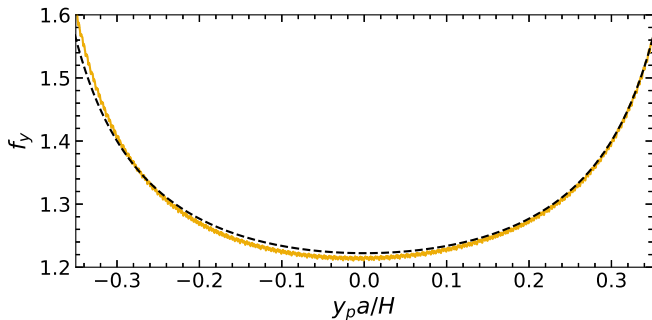


Figure 3. Transverse drag for a particle translating with a small slip velocity (slip Reynolds number $\text{Re}_V = 0.05$) across the channel in a stagnant fluid. Solid curve shows simulation results, dashed curve is calculated from Eq. (19).

increasing Re_G the lift-to-drag ratio increases quickly when $\text{Re}_G \ll 1$ and then shows a weak nonlinear growth. The simulation data are compared with calculations from Eq. (A4), which is the Saffman formula derived for small Re_G . It can be seen that the Saffman formula fits well the simulation data obtained at $\text{Re}_G \ll 1$, but strongly overestimates results at larger Re_G . Also included in Fig. 2 are calculations made using

$$C_l = 0.343\text{Re}_G^{1/2} - 0.106\text{Re}_G \quad (18)$$

obtained by fitting our data in the range $\text{Re}_G \leq 2$. The first term here coincides with the Saffman lift $\bar{C}_l^{S_a}$, and the second, linear in Re_G , term is associated with a correction for finite Re_G .

We now turn to the correction factor to the transverse drag f_y , which depends not only on Re_G , but also on a/H and y_p due to the wall effect. To obtain $f_y = F_y/V_y$ as a function of y_p we place a particle at $y = 0.4$, apply a small vertical force F_y , and then measure V_y along the trajectory. In these simulations we fix $\text{Re}_G = 0$, i.e. perform measurements in a stagnant fluid since at finite Re_G it is difficult to distinguish between the transverse drag and the lift force arising when the particle moves in the y -direction. We stress, however, that the effect of H/a on f_y is stronger than that of Re_G . Consequently, the qualitative features of the f_y curves at finite Re_G are the same, and the quantitative difference from the case of $\text{Re}_G = 0$ should be insignificant. Fig. 3 shows f_y plotted as a function of particle position y_p multiplied by $a/H = 0.05$. It has been earlier proposed that a sensible approximation for f_y in the case of the channel can be simply a superposition of single-wall contributions²⁸

$$f_y = 1 + \frac{1}{H/2a - 1 + y_p} + \frac{1}{H/2a - 1 - y_p}. \quad (19)$$

The calculations from Eq.(19) are also shown in Fig. 3 and we see that the fit is quite good. The function $f_y(y_p)$ takes its minimum value (of ca. 1.22 with our parameters) at the mid-plane, $y_p = 0$. Note that this

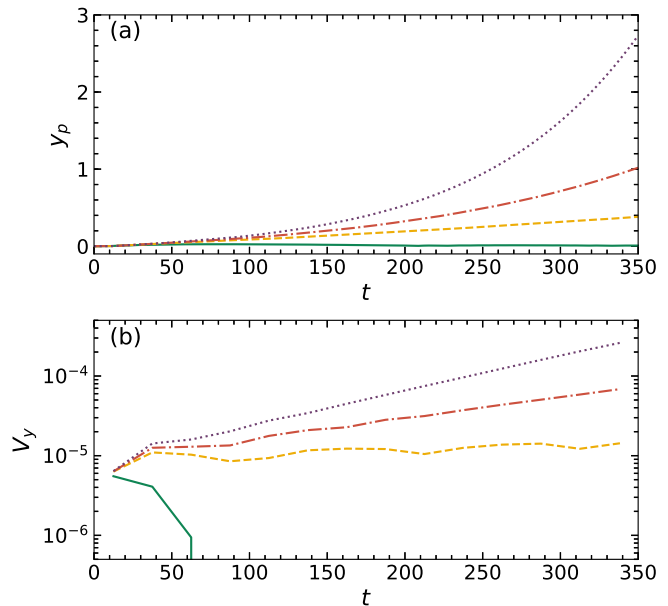


Figure 4. Particle transverse positions (a) and magnitudes of their transverse velocities (b) computed for the Couette flow using $H/a = 20$, $\text{Re}_G = 0.5$ and $\text{St} = 5.6$ (solid), 7.8 (dashed), 8.4 (dashed-dotted), and 8.9 (dotted).

exceeds $f_y = 1$ corresponding to the Stokes drag in an unbounded flow. On approaching the walls f_y increases, which implies that the critical Stokes number St_{cr} given by Eq.(12) also grows. Consequently, inertial migration in the near-wall region can remain stable even when the stability condition is violated in the central part of the channel.

B. Instability for spherical particles in Couette flow

Next we examine the dependence of St_{cr} on Re_G and ρ_p/ρ . In these simulations particles are released at the mid-plane of the channel with a small initial velocity in the x -direction.

Figure 4 show the time dependence of particle trajectories and transverse velocities obtained at $\text{Re}_G = 0.5$. These simulations are made using ρ_p/ρ from 50 to 80, which corresponds to St varying from 5.6 to 8.9. It can be seen that the particle with $\text{St} = 5.6$ remains at the mid-plane, but those with larger St accelerate in the y -direction, demonstrating the instability of the mid-plane equilibrium (Fig. 4(a)). In turn, the velocity V_y reduces for the particle with $\text{St} = 5.6$, but augments exponentially with time if St is larger (Fig. 4 (b)). The simulation data show that at large Stokes numbers the transverse velocity grows with their value.

If similar analysis is made to a variety of simulations performed at different Re_G and ρ_p/ρ , we can find St_{cr} that determines an onset of instability depending on these parameters. Fig. 5 summarizes the simulation re-

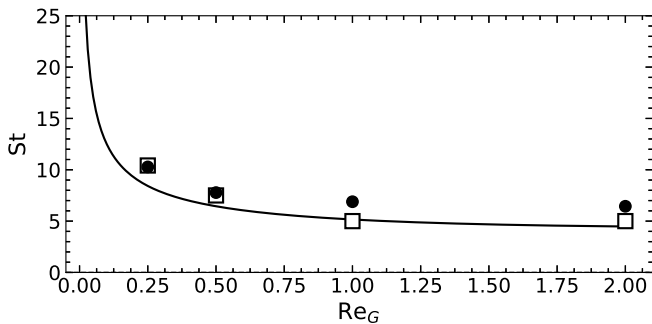


Figure 5. Stability diagram for spherical particles in the Couette flow. Filled circles correspond to the onset of instability obtained in simulations. The solid line is calculated from Eq. (12) using C_l given by Eq. (18) and $f_y = 1.22$. Open squares correspond to simulation data for spheroids.

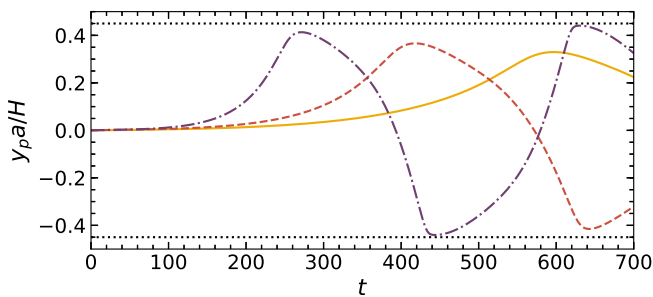


Figure 6. Evolution of transverse positions in Couette flow for the particles with $Re_G = 1$ and $St = 7.4$ (solid), 7.9 (dashed) and 9 (dashed-dotted). Dotted lines indicate contact with the walls.

sults (black circles) obtained for Re_G from 0.25 to 2 and several density ratios ρ_p/ρ in the range from 15 to 200 in the (Re_G, St) plane. Note that the error bars are smaller than the symbol size and, therefore, not shown. Also included is a theoretical, neutral equilibrium, curve calculated from Eq.(12). The calculations are made using $f_y = 1.22$ and C_l given by Eq. (18). An overall conclusion from this plot is that finite Re_G dramatically reduce the value of St_{cr} . We also conclude that the theory reproduces well the qualitative features of the neutral stability curve, although there is some quantitative discrepancy. The discrepancy is always in the direction of smaller St_{cr} than obtained in simulations, which is likely due to underestimated (obtained for $Re_G = 0$) f_y used in theoretical calculations.

We now fix $Re_G = 1$ and monitor the time evolution of y_p at several supercritical St . The results are plotted in Fig. 6. It can be seen that after some interval of time particles discernibly deviate from their equilibrium position $y_p = 0$, and that they move with the acceleration towards the wall indicating unstable equilibrium. However, they slow down in the near-wall region, and, without making contact with the wall, reverse the direction

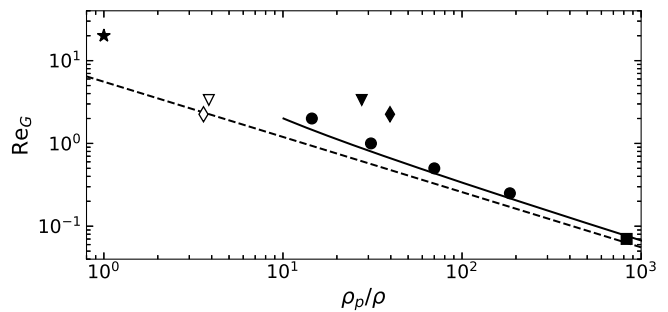


Figure 7. The same as in Fig. 5, but plotted in the $(\rho_p/\rho, Re_G)$ plane. Dashed line is calculated from Eq. (14). The data inferred from earlier results for a pressure-driven flows are shown by filled triangles and diamonds (flat-parallel channels^{32,33}), the star (a circular tube³⁴), and the square (aerosol particles in a square channel³⁵). The earlier data for steady-state trajectories^{32,33} are marked by the open triangle and diamond.

of their motion. The particles then accelerate towards the opposite wall, etc. In other words, we observe the oscillations of particles between channel walls instead of their focusing at the mid-plane. Note that this oscillatory motion depends on St . We see in Fig. 6 that the particles of larger St accelerate faster and oscillate with a smaller period, but larger amplitude. It is well seen that the extrema of y_p become less pronounced and of smaller absolute value on decreasing $St - St_{cr}$. Clearly, the oscillations would disappear at $St = St_{cr}$ and smaller. These observations are, of course, very different from expected for an unbounded shear flow, where the particle would accelerate until the lift force (which reduces with Re_V) becomes equal to the transverse drag. However, for our wall-bounded flow the local St_{cr} depends on y_p . Besides, in addition to the drag and the Saffman lift forces, the neutrally buoyant lift force $F_l^{nb}(y_p)$ (the force F_{ex} in Eq.(15)) is acting on the particles. The latter does not depend on V_y and is caused by inertial hydrodynamic interactions with the walls⁵. Note that although this force is traditionally termed neutrally buoyant, it would be the same for particles of any density. The local St_{cr} increases with the absolute value of y_p , i.e. on approaching the wall, since C_l decreases near the wall³¹, but f_y is much larger near the wall than in the central part of the channel (see Fig. 3). As a result, the particles retard near the wall and V_y tends to zero, so does the Saffman lift force given by (11). One can speculate that particles commence the movement towards an opposite wall instead of immobilization due to F_l^{nb} that is directed away from the wall⁵. They are pushed back to the mid-plane, but since the equilibrium there is unstable, continue to migrate until approach the wall.

Similar oscillatory trajectories have been found in simulations of neutrally buoyant³⁴ and heavy particles^{32,33,35} migrating in pressure-driven flows, but no attempt has been made to connect these results to the equilibrium instability. In Fig. 7 the data and the theoretical cal-

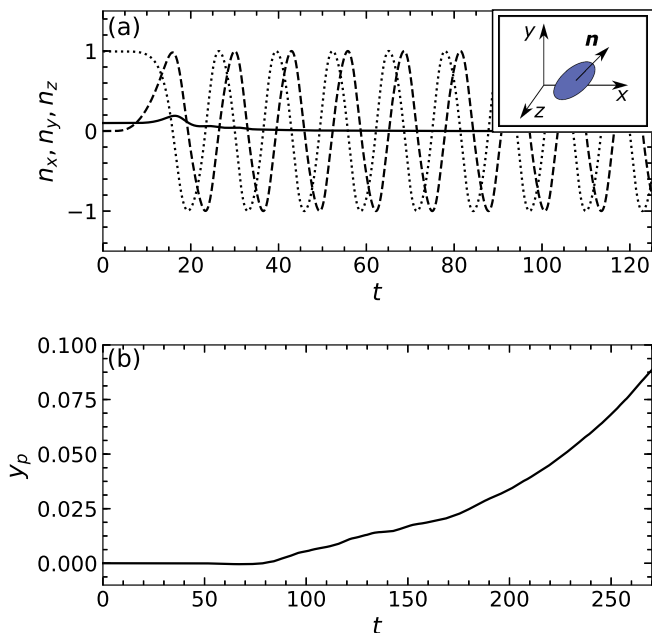


Figure 8. Components of (a) the orientation vector n_x (dotted), n_y (dashed), n_z (solid) and (b) the transverse position of the prolate spheroid in the supercritical regime at $\text{Re}_G = 0.5$ and $\text{St} = 7.8$.

culuation are reproduced from Fig. 5, but plotted in the $(\rho_p/\rho, \text{Re}_G)$ plane and in a log-log scale. They are compared with the above mentioned simulation data obtained for pressure-driven flows and with another calculation, made from Eq.(14). It can be seen that Eq. (12) provides quite good fit of our simulation data, but Eq.(14) underestimates Re_{cr} . We also conclude that earlier data for heavy particles in oscillatory regimes (filled symbols) always either fall into the instability region of a diagram or coincide with its onset. However, the data for steady-state trajectories (open symbols) fall into the stability region. Finally, we remark that the neutrally buoyant particles in an unstable equilibrium³⁴ correspond to $\text{Re}_G \simeq 20$, which is close to the values at which the Segre-Silberberg equilibrium position disappears, leaving only the inner annulus^{10,12}. Therefore, one can speculate that the particle inertia and the Saffman lift force may be important for interpreting this phenomenon too.

C. Translational instability for spheroids

Our theory and above simulation results refer to spherical particles. Here we report some simulation data showing that our model could be suitable for spheroid particles too.

We investigate prolate spheroids of a polar radius b and an equatorial radius a . In all simulations we use

$H/b = 20$ and aspect ratio $b/a = 2$. We define

$$\text{Re}_G = \frac{Gb^2}{\nu}, \quad \text{St} = \frac{2\rho_p Ga^2}{9\mu} = \frac{2\rho_p}{9\rho} \left(\frac{a}{b}\right)^2 \text{Re}_G. \quad (20)$$

and fix $\text{Re}_G = 0.5$ and $\text{St} = 7.8$. The spheroid is initially located at the mid-plane with some small inclination relative to x -axis and move with V_x . The time evolution of the symmetry vector $\mathbf{n} = (n_x, n_y, n_z)$, which characterizes the particle orientation in the channel, is illustrated in Fig. 8(a). We see that after some time a stable tumbling motion is established. This observation is in agreement with prior work¹⁴. Simultaneously, the spheroid migrates in the y -direction with a growing with time velocity as seen in Fig. 8(b). This is exactly what we have observed for spheres (cf. Fig. 4(a)). We have performed additional simulations using several Re_G and St . The results are included in Fig. 5 and indicate that the onset of instability for our spheroid particles is very close to that for the spheres.

We have already mentioned some simulation studies^{13–16} of transitions between different rotational regimes of spheroids. However, these studies addressed the case of $\text{Re}_G \gg 1$ and used fixed coordinates, which implies that rotational and translational motions are decoupled. In our work we have not fixed the spheroid position and found that the instability can occur at much smaller Reynolds numbers, thanks to the Saffman lift force.

VI. CONCLUSION

We have demonstrated theoretically that migration of inertial spherical particles in a shear flow becomes unstable, thanks to the Saffman lift force. It is shown that when their Stokes number exceeds the critical value, inertial particles migrate with an exponential acceleration. Lattice Boltzmann simulations of the critical Stokes numbers generally validate our analysis. Simulations also show that our simple theoretical model is also applied for prolate spheroids, and that the lift-induced instability of spheroid motion occurs approximately at the same Stokes numbers as for spheres.

ACKNOWLEDGMENTS

This work was supported by the Ministry of Science and Higher Education of the Russian Federation. We also acknowledge a partial financial support of by the Deutsche Forschungsgemeinschaft (DFG) under Project-ID 416229255 / SFB 1411 and FOR2688, grant HA4382/8-1.

DATA AVAILABILITY

The data that support the findings of this study are available within the article.

Appendix A: Calculation of the lift force on a migrating particle

In this Appendix, we derive the formula for the Saffman lift force on a particle migrating in the neutral-stability regime.

In his pioneering work Saffman³ calculated a lift force on a sphere moving in unbounded shear flow $\mathbf{U} = y\mathbf{e}_x$ with a constant velocity $\mathbf{V} = V_x\mathbf{e}_x$ parallel to the flow, using the method of matched asymptotic expansions. In the inertial coordinate system associated with the particle, $\mathbf{X} = (X, Y, Z) = \mathbf{x} - \mathbf{x}_p$, the unperturbed flow reads

$$\mathbf{U} - \mathbf{V} = (Y - V_s)\mathbf{e}_x, \quad (\text{A1})$$

where $V_s = V_x - y_p$ is particle slip velocity.

The problem was solved in a strong shear limit, when the shear-based and slip-based particle Reynolds numbers satisfy the condition

$$\text{Re}_V \ll \text{Re}_G^{1/2} \ll 1. \quad (\text{A2})$$

Condition (A2) means that the linear flow dominates over the slip velocity in the outer region of the flow where $Y \sim \text{Re}_G^{-1/2}$. Therefore, far from the particle the unperturbed flow is $\mathbf{U} - \mathbf{V} \simeq Y\mathbf{e}_x$ and the disturbance induced by the particle velocity \mathbf{u} is governed by the Oseen-like equations,

$$\text{Re}_G \left(Y \frac{\partial \mathbf{u}}{\partial X} + u_y \mathbf{e}_x \right) + \nabla p - \nabla^2 \mathbf{u} = 6\pi \mathbf{F}_p \delta(\mathbf{X}). \quad (\text{A3})$$

Here, the terms in the brackets are the Oseen-like inertial terms, $\delta(\mathbf{X})$ is the delta-function, so that the particle effect is approximated by the point force \mathbf{F}_p exerted by the particle on the fluid. For a particle moving with constant slip velocity V_s this force is equal and opposite to the drag on the particle, $\mathbf{F}_p = -F_{dx}\mathbf{e}_x$. Therefore, the lift force is proportional to the drag, and the ratio of the two forces is³

$$C_l^{Sa} = \frac{F_l^{Sa}}{F_{dx}} = 0.343 \text{Re}_G^{1/2} \quad \text{for} \quad \text{Re}_G \ll 1. \quad (\text{A4})$$

Equations (A3) and (A4) are usually written in terms of the slip velocity V_s , since $F_{dx} = -V_s$ for the steady case at $\text{Re}_V, \text{Re}_G \ll 1$.

In our case the situation is different, since the particle accelerates in the streamwise direction and migrates in the transverse direction. We consider the flow using a non-inertial coordinate system translating with the particle, $\mathbf{X} = (X, Y, Z)$.¹⁷ The unperturbed flow around the particle then reads

$$\mathbf{U} - \mathbf{V} = Y\mathbf{e}_x - (V_x - y_p)\mathbf{e}_x - V_y\mathbf{e}_y. \quad (\text{A5})$$

For the neutral-stability regime, the streamwise component of the force \mathbf{F}_p can be found by using Eqs. (4), (8), while the transverse forces are balanced, and hence $\mathbf{F}_p = -\text{St}V_y\mathbf{e}_x$. Since the force is constant the disturbance flow is steady. Assuming that Re_V, Re_G satisfy the condition (A2), we can neglect the last two terms in (A5) in the outer region. Therefore, the disturbance velocity \mathbf{u} in our case is governed by the momentum equation similar to Eq. (A3), with the drag force F_{dx} replaced by $\text{St}V_y$. The lift force on the particle in the neutral stability regime is then given by

$$F_l^{Sa} = C_l^{Sa} \text{St}V_y \quad \text{as} \quad \text{Re}_G \ll 1. \quad (\text{A6})$$

REFERENCES

- ¹G. Segre and A. J. Silberberg, "Behaviour of macroscopic rigid spheres in Poiseuille flow. Part 1." *J. Fluid Mech.* **14**, 115–135 (1962).
- ²D. Stoecklein and D. Di Carlo, "Nonlinear microfluidics," *Anal. Chem.* **91**, 296–314 (2018).
- ³P. G. T. Saffman, "The lift on a small sphere in a slow shear flow," *J. Fluid Mech.* **22**, 385–400 (1965).
- ⁴B. Ho and L. Leal, "Inertial migration of rigid spheres in two-dimensional unidirectional flows," *J. Fluid Mech.* **65**, 365–400 (1974).
- ⁵P. Vasseur and R. G. Cox, "The lateral migration of a spherical particle in two-dimensional shear flows," *J. Fluid Mech.* **78**, 385–413 (1976).
- ⁶D. Di Carlo, "Inertial microfluidics," *Lab on a Chip* **9**, 3038–3046 (2009).
- ⁷P. Shi and R. Rzehak, "Lift forces on solid spherical particles in wall-bounded flows," *Chem. Eng. Sci.* **211**, 115264 (2020).
- ⁸K. Hood, S. Kahkeshani, D. Di Carlo, and M. Roper, "Direct measurement of particle inertial migration in rectangular microchannels," *Lab Chip* **16**, 2840–2850 (2016).
- ⁹A. J. Fox, J. W. Schneider, and A. S. Khair, "Dynamics of a sphere in inertial shear flow between parallel walls," *J. Fluid Mech.* **915**, A119 (2021).
- ¹⁰J.-P. Matas, J. F. Morris, and É. Guazzelli, "Inertial migration of rigid spherical particles in Poiseuille flow," *J. Fluid Mech.* **515**, 171–195 (2003).
- ¹¹Y. Morita, T. Itano, and M. Sugihara-Seki, "Equilibrium radial positions of neutrally buoyant spherical particles over the circular cross-section in Poiseuille flow," *J. Fluid Mech.* **813**, 750 (2017).
- ¹²S. Nakayama, H. Yamashita, T. Yabu, T. Itano, and M. Sugihara-Seki, "Three regimes of inertial focusing for spherical particles suspended in circular tube flows," *J. Fluid Mech.* **871**, 952–969 (2019).
- ¹³D. Qi and L.-S. Luo, "Rotational and orientational behaviour of three-dimensional spheroidal particles in Couette flows," *J. Fluid Mech.* **477**, 201–213 (2003).
- ¹⁴H. Huang, X. Yang, M. Krafczyk, and X.-Y. Lu, "Rotation of spheroidal particles in Couette flows," *J. Fluid Mech.* **692**, 369 (2012).
- ¹⁵T. Rosén, M. Do-Quang, C. K. Aidun, and F. Lundell, "The dynamical states of a prolate spheroidal particle suspended in shear flow as a consequence of particle and fluid inertia," *J. Fluid Mech.* **771**, 115–158 (2015).
- ¹⁶T. Rosén, A. Nordmark, C. K. Aidun, M. Do-Quang, and F. Lundell, "Quantitative analysis of the angular dynamics of a single spheroid in simple shear flow at moderate reynolds numbers," *Phys. Rev. Fluids* **1**, 044201 (2016).
- ¹⁷M. R. Maxey and J. J. Riley, "Equation of motion for a small rigid sphere in a nonuniform flow," *Phys. Fluids* **26**, 883–889 (1983).

- ¹⁸P. Bagchi and S. Balachandar, “Effect of free rotation on the motion of a solid sphere in linear shear flow at moderate Re ,” *Phys. Fluids* **14**, 2719–2737 (2002).
- ¹⁹N. Nakagawa, T. Yabu, R. Otomo, A. Kase, M. Makino, T. Itano, and M. Sugihara-Seki, “Inertial migration of a spherical particle in laminar square channel flows from low to high Reynolds numbers,” *J. Fluid Mech.* **779**, 776 (2015).
- ²⁰C. Liu, G. Hu, X. Jiang, and J. Sun, “Inertial focusing of spherical particles in rectangular microchannels over a wide range of Reynolds numbers,” *Lab Chip* **15**, 1168–1177 (2015).
- ²¹I. Lashgari, M. N. Ardekani, I. Banerjee, A. Russom, and L. Brandt, “Inertial migration of spherical and oblate particles in straight ducts,” *J. Fluid Mech.* **819**, 540–561 (2017).
- ²²R. Benzi, S. Succi, and M. Vergassola, “The lattice Boltzmann equation: theory and applications,” *Phys. Rep.* **222**, 145 (1992).
- ²³C. Kunert, J. Harting, and O. I. Vinogradova, “Random-roughness hydrodynamic boundary conditions,” *Phys. Rev. Lett.* **105**, 016001 (2010).
- ²⁴A. J. C. Ladd and R. Verberg, “Lattice-Boltzmann simulations of particle-fluid suspensions,” *J. Stat. Phys.* **104**, 1191 (2001).
- ²⁵F. Janoschek, F. Toschi, and J. Harting, “Simplified particulate model for coarse-grained hemodynamics simulations,” *Phys. Rev. E* **82**, 056710 (2010).
- ²⁶F. Janoschek, J. Harting, and F. Toschi, “Towards a continuum model for particle-induced velocity fluctuations in suspension flow through a stenosed geometry,” *Int. J. Modern Physics C* **25**, 1441013 (2014).
- ²⁷A. L. Dubov, S. Schmieschek, E. S. Asmolov, J. Harting, and O. I. Vinogradova, “Lattice-Boltzmann simulations of the drag force on a sphere approaching a superhydrophobic striped plane,” *J. Chem. Phys.* **140**, 034707 (2014).
- ²⁸E. S. Asmolov, A. L. Dubov, T. V. Nizkaya, J. Harting, and O. I. Vinogradova, “Inertial focusing of finite-size particles in microchannels,” *J. Fluid Mech.* **840**, 613–630 (2018).
- ²⁹T. V. Nizkaya, E. S. Asmolov, J. Harting, and O. I. Vinogradova, “Inertial migration of neutrally buoyant particles in superhydrophobic channels,” *Phys. Rev. Fluids* **5**, 014201 (2020).
- ³⁰M. Hecht and J. Harting, “Implementation of on-site velocity boundary conditions for d3q19 lattice Boltzmann simulations,” *J. Stat. Mech. Theory Exp.* **2010**, P01018 (2010).
- ³¹E. S. Asmolov, “Dynamics of a spherical particle in a laminar boundary layer,” *Fluid Dynamics* **25**, 886–890 (1990).
- ³²A. S. Jebakumar, K. N. Premnath, and J. Abraham, “Lattice Boltzmann method simulations of Stokes number effects on particle trajectories in a wall-bounded flow,” *Computers & Fluids* **124**, 208–219 (2016).
- ³³L. Zhang, A. S. Jebakumar, and J. Abraham, “Lattice Boltzmann method simulations of Stokes number effects on particle motion in a channel flow,” *Phys. Fluids* **28**, 063306 (2016).
- ³⁴X. Shao, Z. Yu, and B. Sun, “Inertial migration of spherical particles in circular Poiseuille flow at moderately high Reynolds numbers,” *Phys. Fluids* **20**, 103307 (2008).
- ³⁵S. Qian, M. Jiang, and Z. Liu, “Inertial migration of aerosol particles in three-dimensional microfluidic channels,” *Particulology* (2020).